

Soils with swelling potential - Proposal of a final state formulation within an implicit integration scheme and illustrative FE-calculations

H. Heidkamp*

SOFiSTiK AG

Bruckmannring 38, D-85764 Oberschleißheim, Germany

e-mail: Holger.Heidkamp@sofistik.de

C. Katz

SOFiSTiK AG

Bruckmannring 38, D-85764 Oberschleißheim, Germany

e-mail: Casimir.Katz@sofistik.de

Key words: swelling of soils, final-state formulation, Backward-Euler integration scheme, line-search

Abstract

The swelling phenomenon of soils is related to a transition of contents of anhydrite to gypsum and/or adsorption of water to in-situ clay minerals (corrensites). Remarkable - and important from a geotechnical point of view - is the fact that both processes condition an immense increase in volume. Expansion of soil due to swelling actually has caused considerable damage to tunnels in the past.

Unfortunately, numerical simulations of the final state swelling effect by means of the FE-method often suffer from instable, oscillating behavior of the solution. To date, a common approach for considering the arising swelling strains is the "initial stress method", where nodal forces are generated at each element that experiences swelling. These forces represent the inherent stress resulting from the prevented expansion of the element.

Here, an alternative formulation within a stable implicit integration scheme shall be proposed. The approach uses the concept of strain superposition - therefore it is consistent with the formulation of traditional elasto-plasticity - and combines it with a line search procedure that assures material-level convergence.

Illustrative computations show the realization and benefits of the proposed concept.

1 Introduction

1.1 Swelling mechanism

Relevant for construction engineering purposes basically two swelling mechanisms can be distinguished. The first mechanism, termed “osmotic swelling”, is characteristic for clay minerals. It is typically initiated by unloading of these minerals and can be attributed to the ionic concentration gradient between clay mineral surface and the surrounding pore solution. The second mechanism is of chemical nature and takes place in sulfate rock with anhydrite content. In this context calcium sulfate can exist in two modifications, anhydrite and gypsum. Under the supply of water, anhydrite transforms to gypsum. This process involves a significant increase in volume that amounts to 61% in case of a full transformation of the anhydrite contents.

For both the “osmotic” and the “chemical” process it could be shown that the increase in volume caused by swelling is dependent of the current stress state. This fact is important to note with respect to the development of a constitutive relationship, as described in the following.

1.2 Final state constitutive equation

Based on load-controlled oedometric tests with multiple load steps (Huder-Amberg-experiments) already Grob [3] proposed a one-dimensional relationship, where final state swelling strains are related to the present stress state.

$$\varepsilon_{q,\infty} = -k_q \cdot \log\left(\frac{\sigma}{\sigma_0}\right) \quad (1)$$

k_q = modulus of swelling

σ_0 = equilibrium stress with respect to swelling (initial condition)

Here and in the following we consider *tensile stresses and strains as positive* and *compressive stresses and strains as negative*. The above equation is only valid in the range of compressive stresses. σ_0 defines the maximum compressive stress for which swelling still occurs, i.e. the axial stress that is in equilibrium with respect to swelling. In order to extend the relationship to the full stress range one can introduce a limit stress $\sigma_c < 0$ that corresponds to the maximum swelling strain. Doing so the extended one-dimensional relationship reads

$$\varepsilon_{q,\infty} = -k_q \cdot \begin{cases} 0 & , \sigma \leq \sigma_0 \\ \log(\sigma / \sigma_0) & , \sigma_0 < \sigma < \sigma_c \\ \log(\sigma_c / \sigma_0) & , \sigma \geq \sigma_c \end{cases} \quad (2)$$

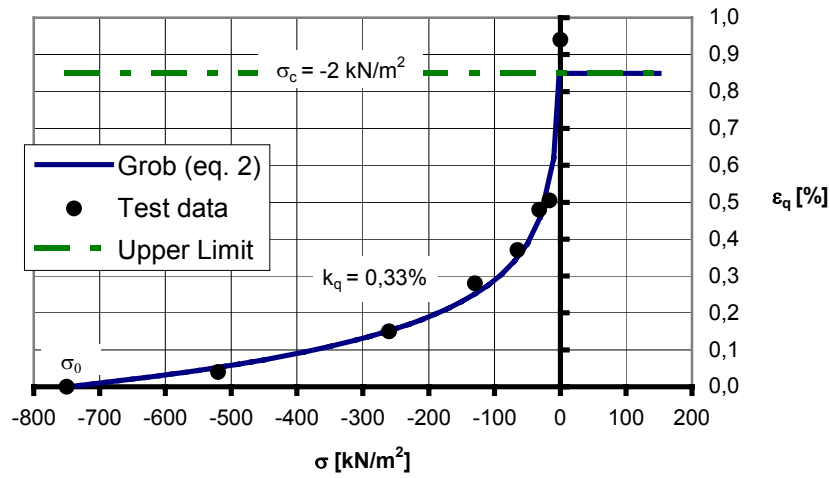


Figure 1: One-dimensional relationship between axial swelling strain and axial stress

Next, the one-dimensional relationship (2) has to be generalized to three dimensions. Here, we restrict our consideration to the isotropic case and basically follow the approach described in Wittke-Gattermann [5]. The vital observation is that the principal swelling strains are essentially dependent of the principal normal stress in the corresponding directions – the stress state in the other directions is of minor relevance. The generalized relationship can be written

$${}^q \varepsilon_{i\infty} = -k_q \cdot \begin{cases} 0 & , \sigma_i \leq \sigma_{i0} \\ \log(\sigma_i / \sigma_{i0}) & , \sigma_0 < \sigma_i < \sigma_c , \\ \log(\sigma_c / \sigma_{i0}) & , \sigma_i \geq \sigma_c \end{cases} \quad (3)$$

$$i = 1..3$$

k_q = modulus of swelling

σ_i = principal normal stresses

σ_{i0} = normal components of the equilibrium state of stress with respect to swelling (initial condition), transformed to the direction of principal normal stresses σ_i

σ_c = (compressive) limit stress that corresponds to the maximum swelling strain

σ_0 represent the stress state that is in equilibrium with respect to swelling. σ_i are the principal normal stresses (resulting from the transformation $T_i \cdot \sigma$). The stresses σ_{i0} are the corresponding components of σ_0 related to the principal directions of σ (i.e. they are obtained via the same transformation $T_i \cdot \sigma_0$). It should be noted that in general σ_{i0} are not equivalent to the principal normal stresses of σ_0 .

2 Implicit formulation (full backward-Euler scheme)

Starting from the concept of strain superposition an implicit formulation of the swelling effect is proposed that is formally consistent with an implicit formulation of ordinary plasticity.

In the context of an incremental strain procedure the global iteration algorithm yields a total strain increment that relates to the last converged equilibrium state (index A). This total strain increment can be split into elastic and swelling strains. For the sake of clarity strain terms related to other material non-linearity than swelling are skipped in the subsequent notation.

$$\begin{aligned}\Delta\boldsymbol{\varepsilon}_t &= \Delta\boldsymbol{\varepsilon}_e + \Delta\boldsymbol{\varepsilon}_q \quad (\dots + \Delta\boldsymbol{\varepsilon}_{pl}) \\ \Delta\boldsymbol{\varepsilon}_q &= \boldsymbol{\varepsilon}_q - \boldsymbol{\varepsilon}_{q,A}\end{aligned}\tag{4}$$

The new stresses write

$$\begin{aligned}\boldsymbol{\sigma} &= \boldsymbol{\sigma}_A + \mathbf{D}\Delta\boldsymbol{\varepsilon}_e \\ &= \underbrace{\boldsymbol{\sigma}_A + \mathbf{D}\Delta\boldsymbol{\varepsilon}_t}_{\boldsymbol{\sigma}_B} - \mathbf{D}\Delta\boldsymbol{\varepsilon}_q\end{aligned}\tag{5}$$

where $\boldsymbol{\sigma}_B$ can be interpreted as the elastic “trial stresses”. Since $\Delta\boldsymbol{\varepsilon}_q$ is a function of $\boldsymbol{\sigma}$ an iterative procedure is required in order to determine $\boldsymbol{\sigma}$. This can be done by defining a residual according to

$$\mathbf{r}_{(k)} = \boldsymbol{\sigma}_{(k)} - (\boldsymbol{\sigma}_B - \mathbf{D}\Delta\boldsymbol{\varepsilon}_q)\tag{6}$$

and applying a truncated Taylor series, so as to produce a new residual.

$$\mathbf{r}_{(k+1)} = \mathbf{r}_{(k)} + \dot{\boldsymbol{\sigma}} + \mathbf{D} \frac{\partial \Delta\boldsymbol{\varepsilon}_q}{\partial \boldsymbol{\sigma}} \dot{\boldsymbol{\sigma}}\tag{7}$$

Here, $\dot{\boldsymbol{\sigma}}$ represents the iterative update of $\boldsymbol{\sigma}_{(k)}$. From the condition that the new residual should vanish we arrive at a rule for updating of the stresses:

$$\dot{\boldsymbol{\sigma}} = - \left(\mathbf{I} + \mathbf{D} \frac{\partial \Delta\boldsymbol{\varepsilon}_q}{\partial \boldsymbol{\sigma}} \right)^{-1} \mathbf{r}_{(k)}\tag{8}$$

$$\boldsymbol{\sigma}_{(k+1)} = \boldsymbol{\sigma}_{(k)} + \dot{\boldsymbol{\sigma}} \quad , \quad k = k + 1\tag{9}$$

A suitable “predictor” stress for the first iteration ($k = 0$) is the elastic trial stress $\boldsymbol{\sigma}_B$. In a case where no swelling occurs for this stress, the residual vanishes and no further iterations are required. In the other case equations (6), (8) and (9) together with the constitutive equations (3) completely define the iterative algorithm in order to obtain the correct stresses, i.e. the stresses that make the residual (6) vanish. The iteration is repeated until, e.g. the Euclidean norm of the residual related to the Euclidean norm of the elastic trial stresses satisfies a specified tolerance.

3 Enhanced algorithm by line-search

3.1 Why enhancing the backward-Euler algorithm?

In order to get an idea of the characteristics of the residual function (6) it is helpful to get back to the one-dimensional case. In particular with an elastic trial stress that is beyond the limit stress, i.e. $\sigma_B > \sigma_c$, the residual function can show a problematic behavior. Assuming fictive values

$$\sigma_0 = -750 \text{ kN/m}^2, \sigma_B = 500 \text{ kN/m}^2, \sigma_c = -10 \text{ kN/m}^2$$

$$k_q = 0.33 \%, E = 3000 \text{ kN/m}^2$$

and evaluating the one-dimensional form of residual function (6) yields:

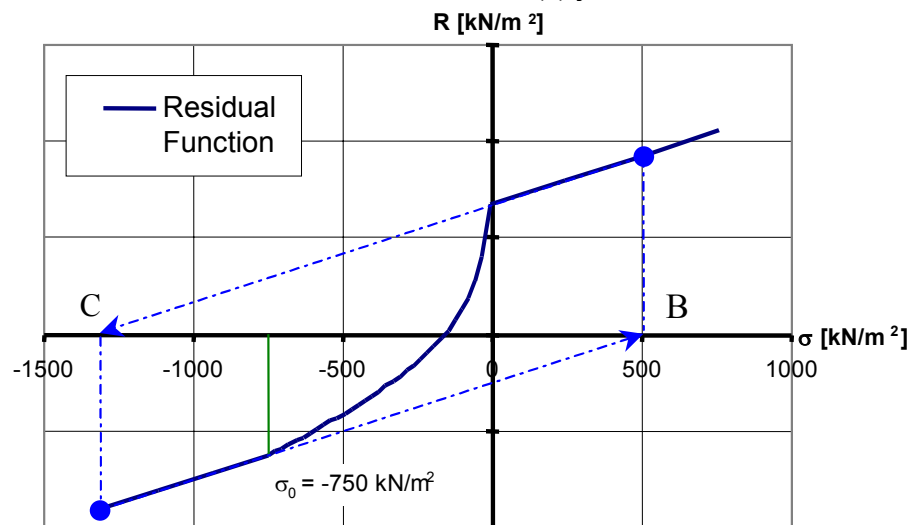


Figure 2: Residual function and standard iterative procedure with tensile elastic trial stress

As is pictured in Figure 2 the standard iteration procedure derived in the previous chapter fails to converge for such a case. For the present example the iterations actually end up in a closed cycle: Stress is taken from point B to C in the first iteration step, hereon the second loop “corrects” the stress back to point B and so on – iterations go on forever without approaching the null of the residual function. Clearly, such a behavior is not desirable and measures have to be taken to avoid a situation like this.

3.2 The line-search concept and its integration into the backward-Euler iterative scheme

The illustrated characteristics principally hold for the three-dimensional case, as well. Therefore, the objective is to enhance the present backward-Euler procedure by some general algorithm that assures convergence. To this end the authors employed an adapted line-search algorithm in combination with the already pictured iterative procedure. Advantages of this approach are, besides the general formulation, the straight-forward integration of the line-search concept into the iterative scheme and the fast convergence. Subsequently, the application of the line-search concept to the present problem shall be outlined.

The objective of a line-search could be described as “finding the best solution in the current search direction”. For this purpose, the iterative stresses (=”search direction”) are scaled by means of a factor.

$$\boldsymbol{\sigma}_{(k+1)} = \boldsymbol{\sigma}_{(k)} + \eta \cdot \dot{\boldsymbol{\sigma}} \quad (10)$$

In equation (10) η must be thought of as the only variable while the stress state of the previous iteration $\boldsymbol{\sigma}_{(k)}$ and the “search direction” $\dot{\boldsymbol{\sigma}}$ remain fixed. We are now looking for the value of η that leads to “smallest” possible $\mathbf{r}_{(k+1)}$. In analogy to a line-search concept applied to the global iterations on the structural level, where the scaling factor η is determined from the condition of minimizing the potential energy [1]– here, we arrive at the condition

$$s(\eta) = \dot{\boldsymbol{\sigma}}^T \mathbf{r}(\eta) = 0. \quad (11)$$

Finding the null of the function s is an iterative process itself. Let us assume that we have computed the residual vector (corresponding to $\eta = 0$) and the stress update according to equations (6) and (8) within the k^{th} iteration. Then the product (11) is computed and stored. Next, in a first step, we would apply the standard update ($\eta = 1$), recompute the residual and then evaluate (11) again. At this stage, we have obtained two pairs of values:

η	$s(\eta)$
0	s_0
1	s_1

From these values a new “guess” of η can be determined by means of some method of inter- or extrapolation. This procedure is continued until condition (11) is satisfied within a specified margin.

Concerning the interpolation the authors found higher order methods to be rather unstable in this context, which can be attributed to the non-smooth behavior of the residual function. Therefore a linear approach is strictly recommend. Additionally, the maximum value of η should be restricted in order to avoid unstable extrapolation.

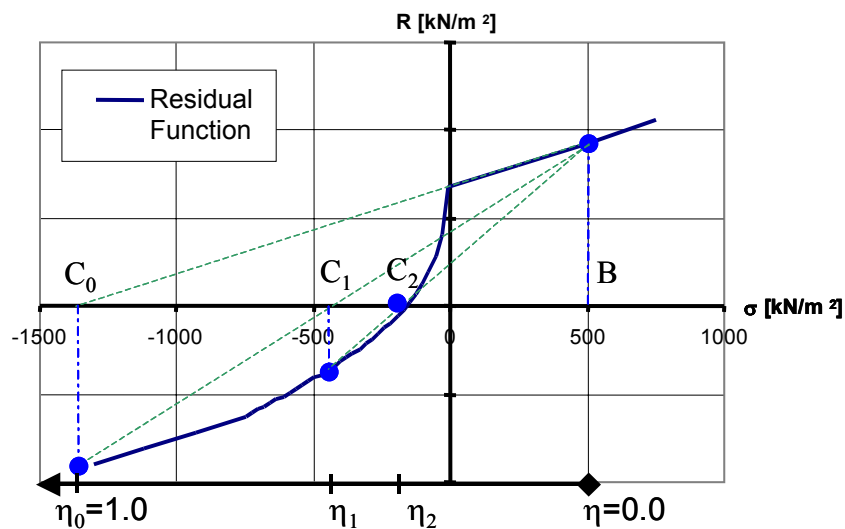


Figure 3: Illustration of the introduced line-search algorithm

Again, it is illustrative to consider the one-dimensional case. It should be noted that for this case – since there is only one possible search direction – the residual can be driven to zero just by means of the line search. This, however, generally does not hold for the three-dimensional case where the right search direction is not known in advance – hence updating of the direction will be required.

The additional expenses of the line-search iterations are rather low since the residual has to be evaluated for the backward-Euler iterations anyway – the line-search can smoothly be integrated into the backward-Euler iterative process.

4 Illustrative numerical simulations

The concept that has been outlined in the previous sections was implemented into the commercial geotechnical FE program TALPA. TALPA was used for subsequent numerical simulations.

First, by means of a simple reproducible example the functionality of the implemented algorithm shall be tested. To this end we simulate the behavior of a specimen during Huder-Amberg testing by applying a corresponding loading sequence to a single quadrilateral element of thickness 1 m under plane strain conditions. Lateral movements of all four nodes are restricted. While the two upper nodes are free to move in vertical direction (= direction of loading) the lower nodes are fixed (see Figure 4). The element's vertical extension is chosen to 1 m – so the resulting vertical displacement equals the strain in loading direction. Starting from an initial compressive loading with $P=5000\text{ kN/m}$ (corresponding to σ_0) the load is stepwise reduced up to a tensile stressing of the element of $P=-1000\text{ kN/m}$. For each of these “unloading steps” swelling is activated and corresponding swelling strains/ displacements are computed.

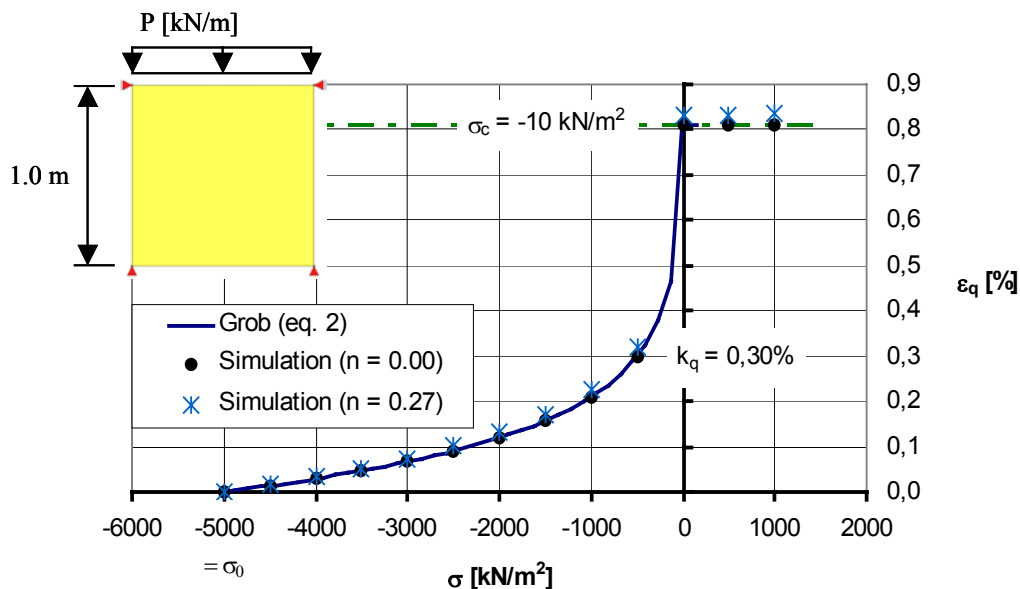


Figure 4: Model geometry and material properties used for the numerical simulation

Setting Poisson's ratio to 0.00 , only stresses in the loading direction can develop – we obtain the one-dimensional case. Therefore, we expect the analytical solution to exactly reproduce Grob's relationship (2). Figure 4 shows that the analytical results indeed meet our expectations. In order to

illustrate the influence of lateral stressing a further analysis with Poisson's ratio chosen to 0.27 is performed. In this case, a (more realistic) full three-dimensional stress state develops within the element (due to constrained lateral movements). Compared to the one-dimensional case the analysis yields somewhat larger swelling strains in loading direction (Figure 4). This increase relates to contributions of the lateral directions, in which – due to unloading – swelling strains develop as well. The lateral swelling strains are coupled with the loading direction via Poisson's ratio (5). It is obvious that calibration of the swelling parameters more realistically should be done on the basis of the second case.

In a second example, the algorithm is used for a more comprehensive engineering problem. The subsequently introduced model approximately represents a section of the Belchentunnel which is part of the N2 national road in Switzerland. The tunnel partly runs through contents of clayey soil with swelling potential, the coverage above the crown in these regions ranges from 100 m to 200 m. The Belchentunnel was released for traffic in 1971. Already during the building process very significant swelling phenomena occurred, therefore, the tunnel base was reinstalled with reinforced concrete of a thickness of 0.85 m. Additionally, several sections along the base were provided with measuring devices for the radial pressures transferred from the soil to the concrete.

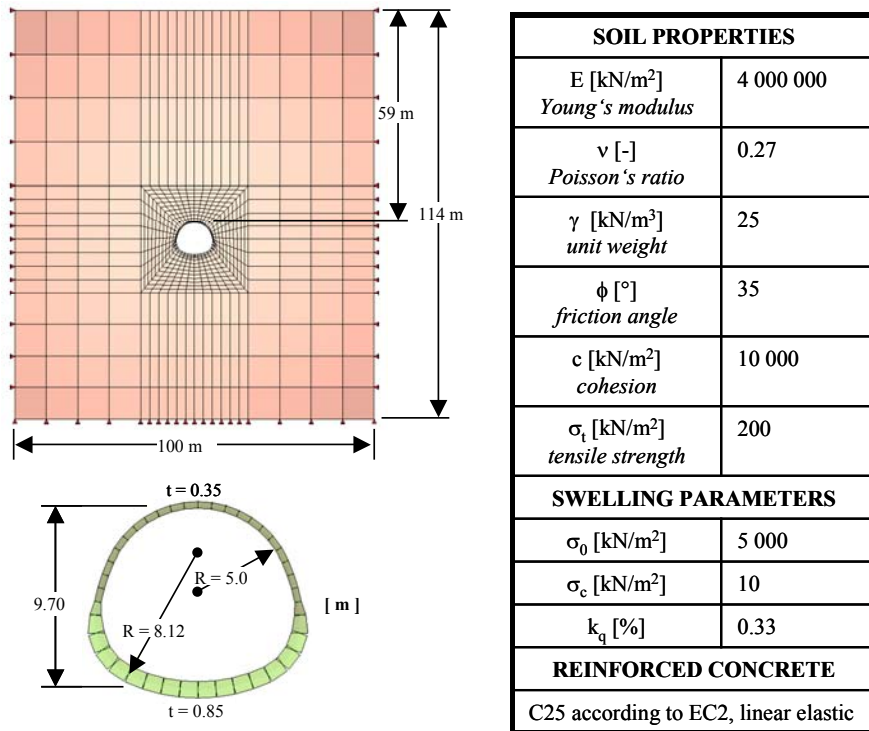


Figure 5: Model geometry and material properties used for the numerical simulation

For the analysis we consider a depth of coverage above the crown of 200 m. Furthermore, it is assumed that the initial stress state in-situ (prior to the construction measure) is in equilibrium regarding swelling, i.e. the swelling strains relating to that stress state already have developed by the time of construction. Due to the deep location of the tunnel tube a strong development of swelling strains can be expected: The deeper the tunnel is situated the more significant is unloading due to excavation – hence, larger swelling strains can arise (compare (1)). The basic model geometry and employed soil properties can be seen from Figure 5. The effect of the remaining coverage that is not

captured in the model is represented by an evenly distributed vertical load acting on the upper model boundary. The analysis is carried out under plane strain conditions.

For the present example it is illustrative to look at the impact of swelling on the concrete lining. If swelling is not taken into account, the analysis shows just a moderate straining of the lining, represented by the bending moment distribution and the corresponding displacements in Figure 6. In fact, the tube is – due to the rather good soil properties – mainly loaded by self-weight. After full development of swelling strains, however, the analysis reveals significantly different results. While tunnel crown and base experience in particular vertical inward-looking movements the side wall regions are pushed outwards (Figure 6). This deformation causes significant bending straining of the lining. It becomes evident in particular for the tunnel base where the extreme values change from +24 kNm to -5700 kNm in the two contrasted cases! Clearly, a tunnel tube which is designed on the basis of an analysis that does not take swelling sufficiently into account is very unlikely to withstand the arising swelling pressures.

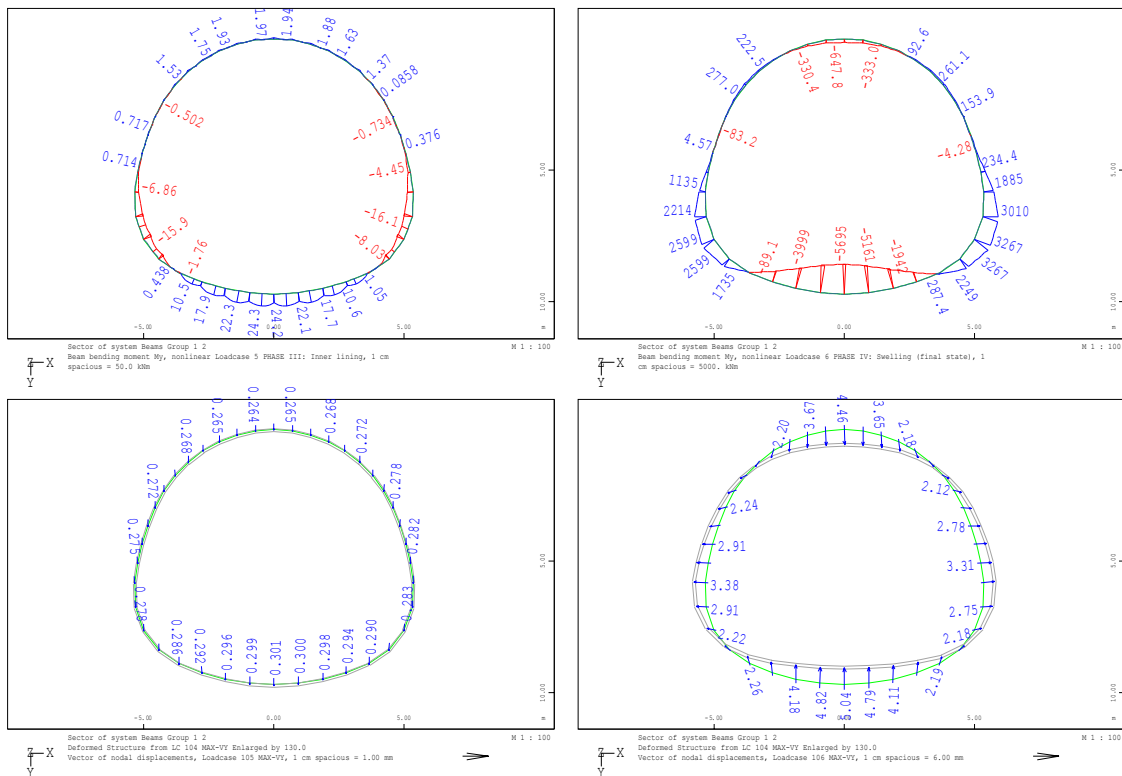


Figure 6: Final stressing of the inner lining without (left) and with (right) consideration of swelling – Moment distribution and corresponding deformation

Insofar the analytical results are qualitatively very well in accordance with observations made in practice: In [4] it is reported that the base of the Belchentunnel, which was originally built with a thickness of 0.45 m, was destroyed along a distance of 500 m due to evolving swelling pressures.

A quantitative assessment of the obtained results is difficult to make and in the present case – due to the approximate character of the model (e.g. uncertainties about the employed swelling modulus k_q as well as lacking information about the influence of the building phases) – not really justified. Nevertheless, by comparing the base pressures that were measured in the considered section in 1972 with the analytical results we find that the order of magnitude of the predicted base pressures is

correct: Base pressures of 1.75 MN/m^2 average up to 3.80 MN/m^2 maximum were measured [4] and the analysis yields values of 1.25 MN/m^2 to about 2.0 MN/m^2 .

5 Conclusive remarks

Based on the three-dimensional extension of Grob's swelling law by Wittke-Gattermann (3) an implicit formulation within a Backward-Euler iteration scheme was proposed. The so-derived algorithm was enhanced by means of a line-search concept, benefits of this concept were illustrated.

Finally, – in order to investigate the functionality of the concept – the presentation was concluded by illustrative computations performed with the geotechnical FE software TALPA in which the proposed concept was implemented. The first analysis, a one-dimensional simulation of a Huder-Amberg testing, yielded the expected response – the run of the theoretical stress – swelling strain relation could be reproduced exactly. The second analysis, an approximate investigation of a section of the Belchentunnel (Switzerland), showed the applicability of the algorithm to practical engineering problems.

6 References

- [1] M. A. Crisfield, *Nonlinear Finite Element Analysis of Solids and Structures, vol. 1: Essentials*, John Wiley & Sons Ltd., Chichester, England (1991).
- [2] M. A. Crisfield, *Nonlinear Finite Element Analysis of Solids and Structures, vol. 2: Advanced Topics*, John Wiley & Sons Ltd., Chichester, England (1997).
- [3] H. Grob, *Schwelldruck am Beispiel des Belchentunnels*, Sitzungsberichte Int. Symposium für Untertagebau, Luzern, Switzerland (1972), pp 99-119
- [4] W. Wittke, *Grundlagen für die Bemessung und Ausführung von Tunnels in quellendem Gebirge und ihre Anwendung beim Bau der Wendeschleife der S-Bahn Stuttgart*, Veröffentlichungen des Institutes für Grundbau, Bodenmechanik, Felsmechanik und Verkehrswasserbau der RWTH-Aachen, Germany (1978).
- [5] P. Wittke-Gattermann, *Verfahren zur Berechnung von Tunnels in quellfähigem Gebirge und Kalibrierung an einem Versuchsbauwerk*, Geotechnik in Forschung und Praxis, Verlag Glückauf GmbH, Essen, Germany (1998), pp. 22-31.
- [6] O.C. Zienkiewicz, R.L. Taylor, *The Finite Element Method*, vol. 2: Solid and Fluid Mechanics, Dynamics and Non-linearity, McGraw-Hill Book Company, London, England (1991).